12th IEA Heat Pump Conference 2017

Transient Acoustic Signatures of the GreenHP with special focus on icing and defrosting

Christph Reichl[a,*], Johann Emhofer[a], Frieder Lörcher[b], Andreas Strehlow[c], Mirza Popovac[a], Peter Wimberger[a], Christian Köfinger[a], Andreas Zottl[a], Thomas Fleckl[a]

[a] AIT Austrian Institute of Technology, Energy Department, Giefinggasse 2, 1220 Wien, Österreich
[b] Ziehl-Abegg SE, Heinz-Ziehl-Straße, 74653 Künzelsau
[c] AKG Verwaltungsgesellschaft, Am Hohlen Weg 31, D 34369 Hofgeismar, Deutschland

Abstract

In the framework of the EU project *GreenHP* a new air-water-heat pump using the natural refrigerant propane is developed. A new compressor concept, heat exchangers produced out of aluminium microchannels attached to efficient air fin structures and a specialized fan have been implemented. The acoustic behaviour is characterized setting a special focus on transient effects during icing and defrosting. For this purpose, a 64-channel acoustic dome is positioned around the heat pump in the climate chamber to acquire space-, time- and frequency resolved microphone data. Measurements are performed for different acoustic shielding of the heat pump. The resulting acoustic directivity and its variation during frosting is correlated to fluid flow and ice aggretion measurements: laser optical methods (particle image velocimetry) and probe techniques (constant temperature anemometry) are used to measure the air velocity both at the air inlet and in the gap between heat exchanger and fan. Computational fluid mechanics is performed to simulate the frosting behaviour based on the measured boundary conditions. For accessing the ice amount a local measuring method is applied based on the fact, that the heat exchanger in the *GreenHP* is positioned horizontally: Below the heat exchanger area, 180 boxes are positioned gathering the water during defrosting. The local ice amount is compared to the simulation results, which are correlated to the acoustic data. Providing these toolsets for development of low noise signature air-to-water heat pumps is important for increasing acceptance of this technology.

Selection and/or peer-review under responsibility of the organizers of the 12th IEA Heat Pump Conference 2017.

Keywords: Air-Water-HeatPump; Acoustics; Icing; De-frosting; Computational Fluid Dynamics; GreenHP; PIV; CTA

* Corresponding author. Tel.: +43-50550-6605; fax: +43-50550-6679.
E-mail address: christoph.reichl@ait.ac.at

1. Introduction

The evaporator unit of the *GreenHP* (see Strehlow et. al. [1] and Reichl et. al. [2]) consists from bottom to top of a horizontal heat exchanger, the air guidance box and the fan (see Figure 1 and 2 left and right). Here, both, experimental and numerical methods are presented, which are used to characterize the air-side of the *GreenHP*. Chapter 2 is focusing on the acoustical measurements (see also Crocker [3] and Gustafsson [4] for investigations on acoustics of heat pumps), which have been performed both in an anechoic room at Ziehl-Abegg (Chapter 2.1, Lörcher et. al. [5] and Angelis et. al. [6]) and a climate chamber at AIT (Chapter 2.2). Methods for characterizing the fluid dynamics are shown in chapter 3, introducing probe (Chapter 3.1) and laser-optical (Chapter 3.2) techniques. This is complemented by a local method to measure ice aggretion (Chapter 3.3). In Chapter 3.4 results from computational fluid dynamics enhanced by an ice aggretion code are compared to the experimental results. Concluding remarks on the air side characterization of the GreenHP are given in Chapter 4.

2. Acoustic Measurements

The acoustic characterization has been performed for the fan mounted on a box in the anechoic chamber (Chapter 2.1) and for the whole evaporator unit (Chapter 2.2). During the measurements in the climatic chamber the compressor (and hence the cooling circuit) and the air handling unit of the climate chamber have been switched off repeatedly for a short time to capture the change in acoustic emissions due to the advancing icing (and blocking) of the evaporator.

Fig. 1. Demo-Setup of the 64 microphone “acoustic dome” positioned around the *GreenHP*. This measuring dome allows for a flexible positioning of the microphones in different distances as all six stands can be changed in height and arranged in varying number and position to each other.

2.1. Acoustic Measurements in the Anechoic Test Room

The tests have been carried out on the large ventilation test rig of Ziehl-Abegg (see Figure 2 mid). This is a combined test rig where airflow characteristic data, electrical data and acoustical data can be compiled

simultaneously, whereby the acoustical data is measured independently on the suction and the pressure side of the fan. The fan is mounted in between the suction and the pressure side centrally of the separation wall. The acoustical measurement method is the envelope surface method under free-field conditions according to standards ISO5801 and AMCA 210-99. On the suction and the pressure side there are each 12 microphones placed on a hemisphere with radius 3 m around the sound source. Both the suction side and the pressure side chambers are cube shaped with a side length of approx. 9 m. On all walls unless the central separation walls, sound absorbers are applied. The test rig is certified to have class 1 accuracy down to 100 Hz. Maximum fan diameter is 1800 mm, maximum airflow is 100000 m³/h and maximum static pressure rise is 3000 Pa. An auxiliary fan system allows it to come to fan duty points with very low static pressure rise.

Fig. 2. (left) Design of the evaporator unit of the *GreenHP* prototype (CAD drawing). In the normal operating mode, the fan (top, visualized in dark) is drawing the air from the bottom through the heat exchanger. On the right side of the drawing the bionic distributor can be seen; (mid) Measuring setup in the anechoic chamber at Ziehl-Abegg, Germany; (right) Setup for the constant temperature anemometry (CTA) measurements. To the right of the *GreenHP*, a fully automated three-axis traversing system is placed to position the CTA probe below the heat exchanger, in the area between heat exchanger and fan and above the fan.

Figure 3 left shows the static pressure rise and the electrical power at a rotation speed of 720 rpm as a function of air volume flow. Out of these measurements, two operating points have been selected. OP1 mimics a situation without icing and hence no additional pressure drop, whereas OP2 would be observed at severe icing, where an additional pressure drop is introduced. The sound power at these operating points are shown in Figure 3 mid (OP1) and right (OP2) both for the pressure and suction side.

2.2. Acoustic Measurements in the Climatic Wind Chamber

64 microphones have been placed in form of a cylindrical grid around the *GreenHP* (see Figure 1). Results differ in the different directions and six representative microphones have been selected to show typical spectra in this work (see Figure 4 top right). The time dependent sound pressure levels of these microphones during icing of the evaporator is shown in Figure 4 bottom right. An increase of around 5 dB for the microphones 35 and 23 can be seen, the positions 2, 26 and 47 only showing a slight variation over time (around 2 dB).

Microphone 52 is placed in the air flow, mainly flow effects being recorded (thus not pure acoustic effects can be observed here). With increasing icing of the evaporator the flow field changes above the fan (recorded by microphone 52), thus a local reduction of the pressure variations can be seen there. The *GreenHP* keeps the rotational speed of the fan constant during icing, increasing sound emission because of increasing rotational speed (as observed for some heat pumps having increasing fan speed for maintaining the power output of the heat pump) is not seen here.

Spectrographic representations for these six acoustic signals in the completely clean (begin) and at severe icing conditions (end of cycle) are depicted in Figure 4 left. Microphone 52 (positioned inside the flow) carries the highest energies, the remaining representative microphones show comparable spectra with varying distribution widths. During icing, the frequency content changes slightly, which can bee seen in Figure 4 left.

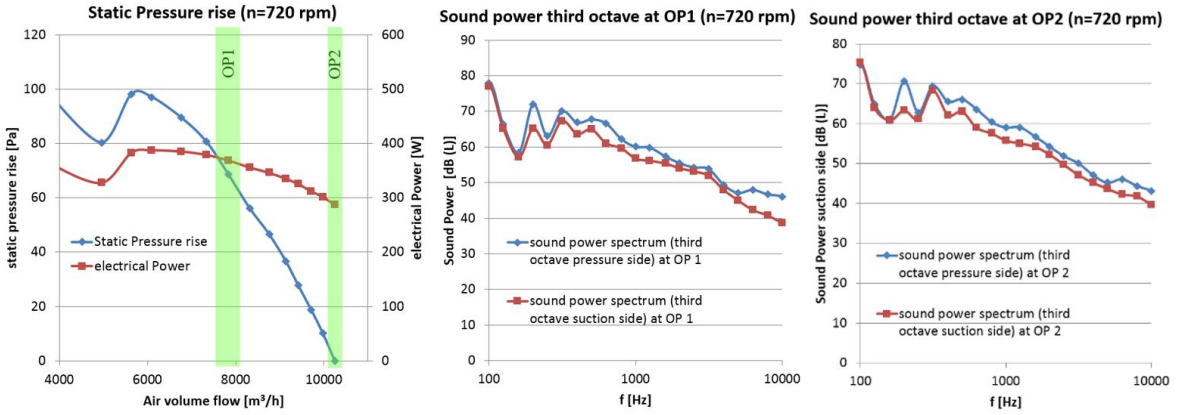

Fig. 3. (left) Static pressure rise at a fan speed of 720 rpm as a function of the air volume flow for the fan used in the *GreenHP* demonstration setup. In green two operating points are marked (OP1 without icing and hence no additional pressure drop, OP2 with severe icing and therefore additional pressure drop); (mid) Sound power at operating point OP1 showing the spectrum at the pressure and suction side; (right) Sound power at operating point OP2.

To acoustically shield the air volume between heat exchanger and fan, two materials from the company *Cellofoam* with a thickness of 40 mm have been attached to the inner surfaces: Absorber 1 is D2600schw/SK-05 and absorber 2 is F800 FR HO/ALG-01/SKN. A comparison of the unshielded *GreenHP* evaporator unit to the units shielded with these two absorber types is given in Figure 5. Analyzing the spectral content of the six microphone positions only slight changes are introduced by attaching the sound absorbing material to the inner surfaces of the air volume between heat exchanger and fan. The majority of the sound waves are emitted by the fan directly and only the part first emitted inwards in direction of the heat exchanger and then transmitted through the heat exchanger or reflected back through the fan is influenced by the sound shielding. Furthermore, changes in the air volume due to the attached material changes slightly the operating point of the fan leading to additional variations in the spectra. It can be concluded, that no significant effect can be observed by adding the sound absorbers at the inner side as described above.

3. Fluid Dynamic Characterization

3.1. Probe Technique – Constant Temperature Anemometry

Constant temperature anemometry (CTA) has been used as a probe based technique to access velocity- and turbulence profiles below the heat exchanger, in the volume between heat exchanger and fan and above the fan. The results were used as boundary conditions for the simulations (shown in Chapter 3.4) and for validating the numerical data. For the measurement of the fan profiles (see Figure 6) data has been recorded along a line through the center of the fan. All other profiles have been captured in a quadrant with the fan center point in one corner (top left corner in the figures) using a 3-axis traversing system placed alongside the *GreenHP* (see Figure 2 right). After allowing the probe to stabilize, 10 seconds of data have been captured with a frequency of 40.000 Hz. The cooling circuit (distributor, compressor) was deactivated during the CTA measurements. Data has been acquired both for a 60% fan control setting (corresponding to around 550 rpm of the fan) and 90% fan control setting (approximately 1250 rpm of the fan) for normal and reversed flow conditions. Beside calculating the velocity magnitude, the frequency content and the turbulence of the flow can be characterized using the CTA technique (see Figures 6-8).

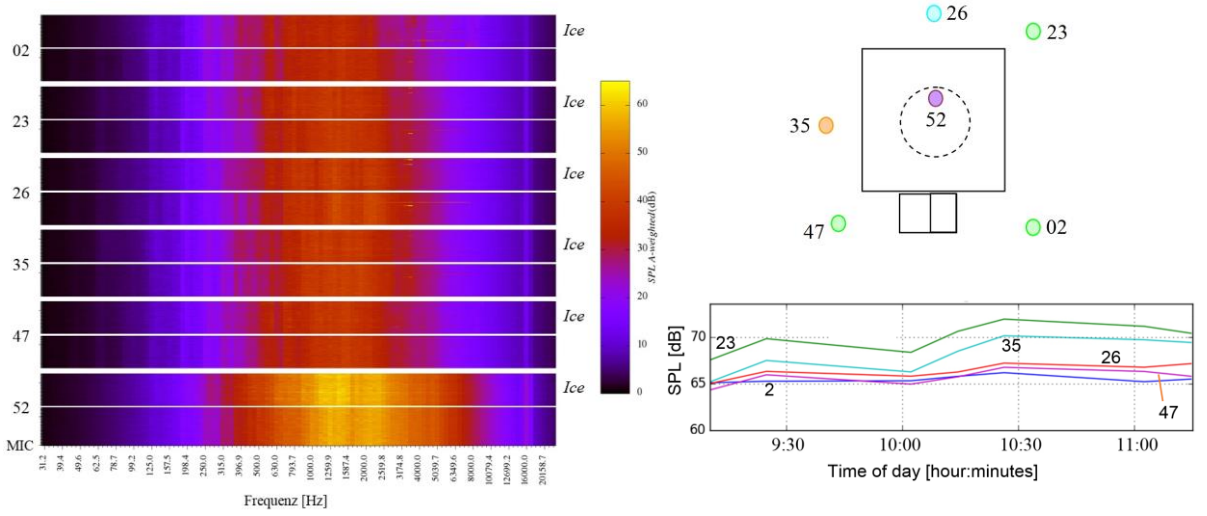

Fig. 4. (left) Spectrogram for six representative microphones (02, 23, 26, 35, 47, 52). The compressor and the ventilation system of the climate chamber have been switched off for some minutes for these measurement to record the acoustic data. For each microphone a spectrum without ice (lower spectrogram) and in the state of severe ice aggretion (upper spectrogram) is shown. The data corresponds to the sound pressure level at the microphone position. Microphone 52 directly placed in the flow is influenced by the flow turbulences; (right top) Microphone positions shown in top view of the *GreenHP*: Mic 26 & 35 are in the lower area (685 mm, 1065 mm above ground), Mic 02 in the middle area (1400 mm), Mic 23 & 47 in the upper area (1860 mm), Mic 52 is placed above the fan (1970 mm); (right bottom) Typical time dependence of the sound pressure level of selected representative microphones. During progressive ice aggretion changes in the sound pressure level can be observed.

Above the fan (see Figure 6) the typical effect of the shear layer can be observed in the normal mode, where air is blown outwards to the top at the outer edge of the fan. In reversed mode this shear layer can be observed

following downstream through the inner air volume (see Figure 7 right) and even below the heat exchanger (see Figure 8c and 8d). In the normal mode (see Figure 7 left and mid) the flow velocity at the different distances above the heat exchanger (13 cm, 27 cm) in the inner volume is becoming more and uniform. Below the heat exchanger the flow is uniform in the normal mode indicating a good distribution of the air flow around the heat exchanger as well (see Figure 8a and 8b top row). The corresponding turbulence levels (see Figure 8a and 8b bottom row) are slightly asymmetric and more pronounced in the center area of the evaporator unit. In reverse mode the jet-like flow field powered by the fan continues below the heat exchanger and a maximum in the center and increased turbulence values in the shear layer remain.

3.2. Laser optical analysis – Particle Image Velocimetry

To facilitate optical flow measurement techniques like Particle Image Velocimetry (PIV), the evaporator unit of the *GreenHP* has been built with transparent surfaces where possible (sides, top). Using PIV, velocity distributions have been recorded on a vertical cut plane between heat exchanger and fan. Figure 9 shows vector plots resulting from cross-correlation data analysis. Seeding particles have been introduced from below the heat exchanger and drawn through the heat exchanger to the fan.

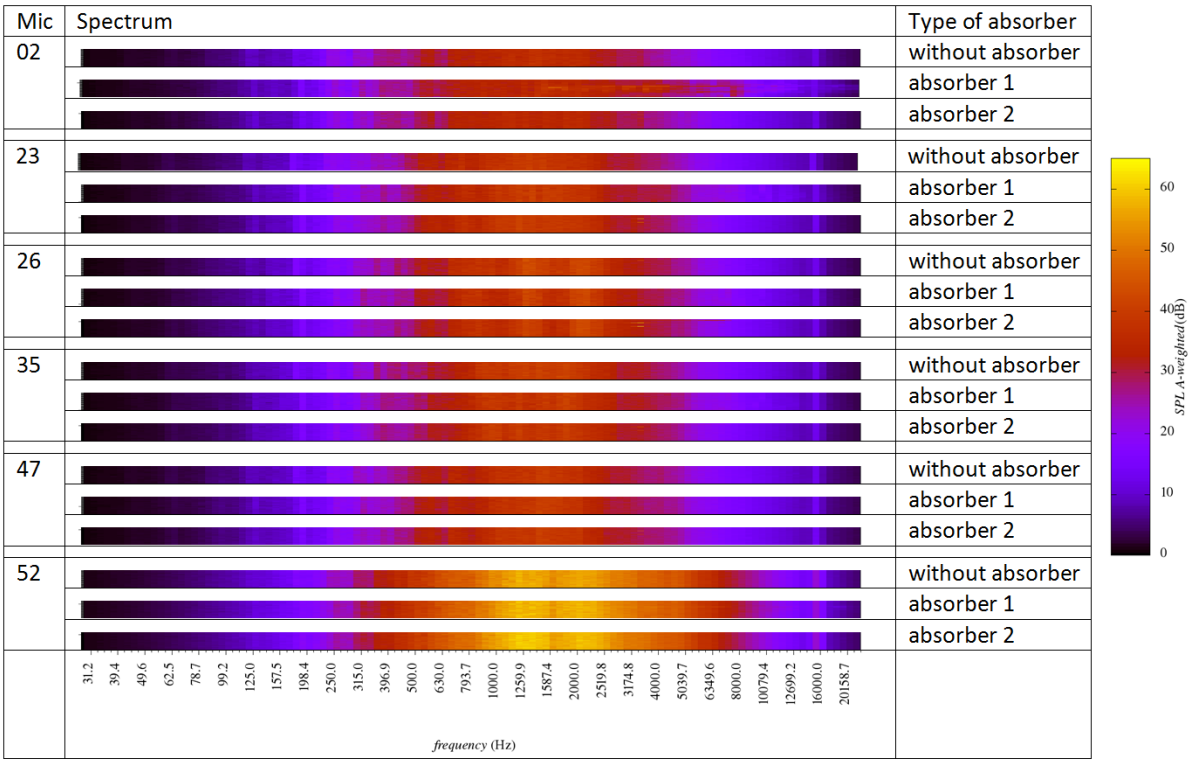

Fig. 5. Comparison of different sound absorption measures in the air volume between heat exchanger and fan for representative microphone positions. A-weighted sound pressure levels at six different recording positions (microphones 02, 23, 26, 35, 47 & 52) are shown in frequency spectra for 3 scenarios: without absorber (top row), absorber material 1 (middle row), absorber material 2 (bottom row).

In the clean state (no ice aggretion), the flow can be approximated by a conic form: the mean flow draws the air from inside the unit equally distributed in direction to the fan (left upper corner in the figures) – only a small recirculation zone remains in the vicinity of the corners. During icing of the evaporator only low velocity flows can be observed in the main part of the volume due to increasing drag. Large circulation zones are observed in the area between heat exchanger and fan as a result.

3.3. Local measurement of Ice Aggretion

The local distribution of aggregated ice in the heat exchanger can be analyzed using weight measurements of water, which is gathered in boxes placed below the heat exchanger (see Figure 10 left). They contain the water, which is dropping down during defrosting of the horizontal heat exchanger. Figure 10 right shows the local water mass and the sums over the columns and rows. It can clearly be seen, that the horizontal distribution (top bar graph in Figure 10 right) is not equal and some rows are more prone to icing than others, which is inline with optical ice detection and points towards a non equal cooling media distribution inside the heat exchanger (taking into account the homogenous distribution of air over the heat exchanger). The vertical distribution (left bar chart in Figure 10 right) shows a typical reduction in water (ice) mass with rising cooling media temperature downstream of the cooling circuit, where more and more cooling media has phase changed from the liquid to the gaseous phase.

3.4. Comparison to numerical methods – Computational Fluid Dynamics

Numerical analysis have been performed using Computational Fluid Dynamics (CFD) using the open-source solver package OpenFoam (Weller et. al. [7]). The discretized equation system consisting of continuity-, momentum and energy-equation is solved applying the finite volume approach. For accessing the ice growth (see also Na et. al. [8], [9], Albert et. al. [10]) the relative humidity has been implemented as a passive scalar field. The model of Hermes et. al. [11] has been chosen for modeling ice growth and prediction of densification. It is based on the fundamental principles of energy and mass conservation. The process of mass and heat diffusion inside the frost layer is treated quasi-stationary and one dimensional and the frost thickness is assumed to be uniform along the surface. Additionally, the model requires satisfaction and applicability of the Lewis-Analogy (see also Popovac et. al. [12], [13] and Reichl et. al. [14]). Figure 11 shows the velocity magnitude on different horizontal surfaces which can be compared to Figure 7 and 8. The typical jet-like flow can be seen in Figure 11 left and right for the reverse operating mode, whereas the uniform distribution in the normal mode is observed in Figure 11 mid. Contour and vector visualization is given in Figure 12 for the clean and blocked state (compare to Figure 9) showing the recirculation flow as observed in the experiment. The frost growth (Figure 12 right) can be linked to water mass measurements presented in Figure 10 right showing the numerical defined *alphaFrost* value, representing the volume fraction occupied by frost.

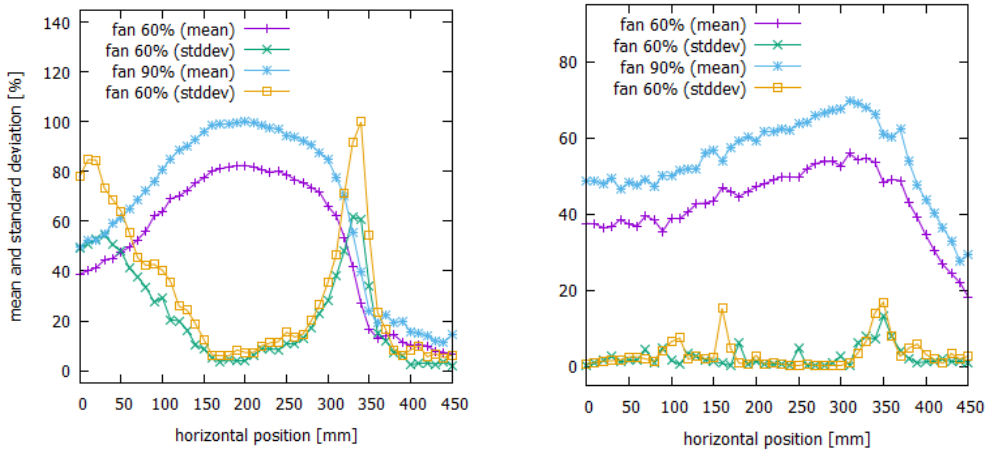

Fig. 6. Mean values and standard deviation of the CTA signal correlated to the mean velocity and turbulence levels 10 cm above the fan, respectively. These values are given for two different settings of the fan control setting: 60% corresponding to around 550 rpm and 90% (1250 rpm). (left) The fan is operated in normal mode drawing air flow from below the heat exchanger; (right) The fan is operated in reverse mode blowing the air from top towards the heat exchanger.

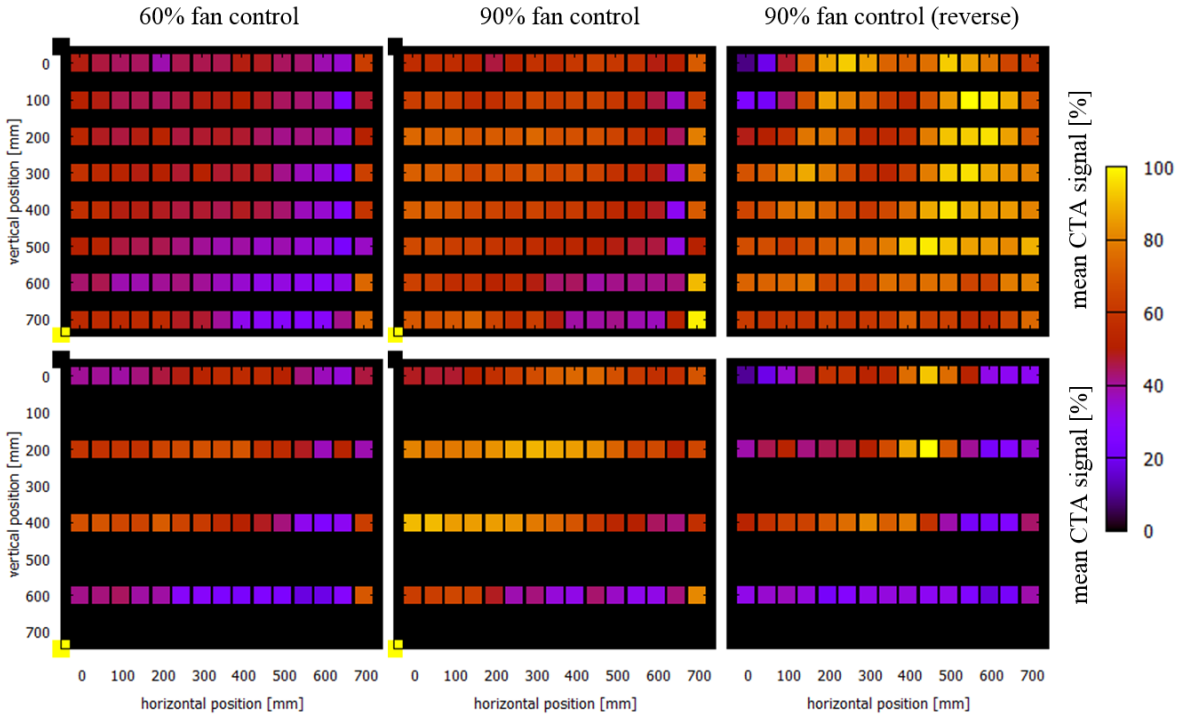

Fig. 7. Comparison of the mean CTA signal (correlated to mean velocity) 13 cm above (upper row) and 27 cm above (lower row) the heat exchanger in the volume between heat exchanger and fan. The left upper corner always corresponds to the center of the fan; only one quadrant of the area below the fan has been measured corresponding to the symmetry of the setup. Data is shown for three settings on the fan: (left row) normal mode 60% fan control; (middle row) normal mode 90% fan control; (right row) reverse mode 90% fan control.

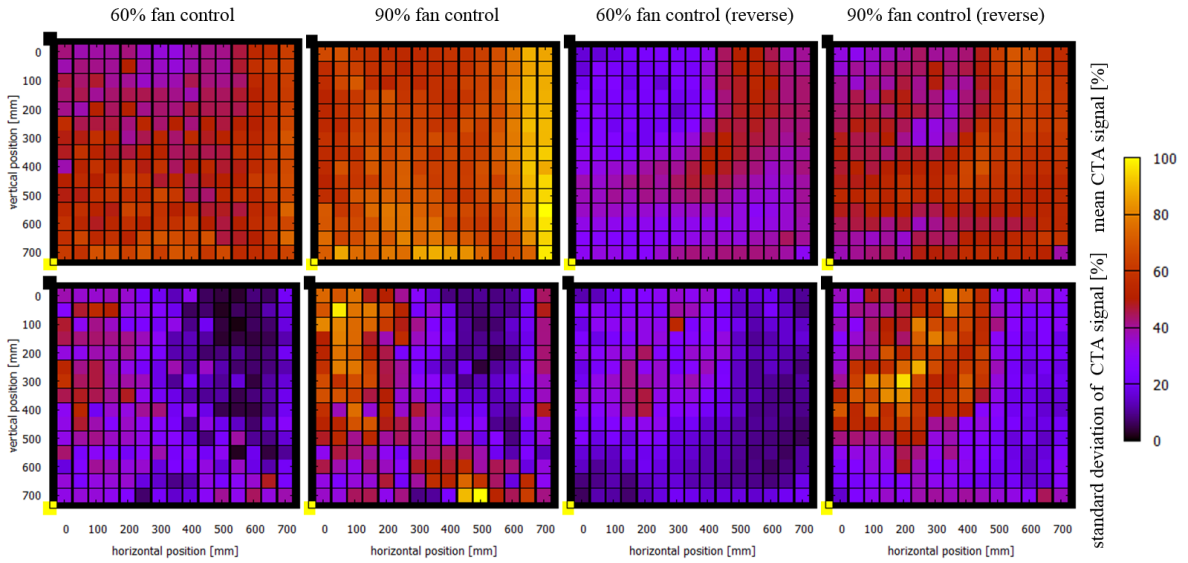

(a) (b) (c) (d)

Fig. 8. Comparison of mean CTA signal (corresponding to mean velocity, upper row) and standard deviation of CTA signal (corresponding to turbulence levels, lower row) 10 cm below the heat exchanger. Data is shown for four different settings from left to right: (a) normal mode 60% fan control, (b) normal mode 90% fan control, (c) reverse mode 60% fan control and (d) reverse mode 90% fan control.

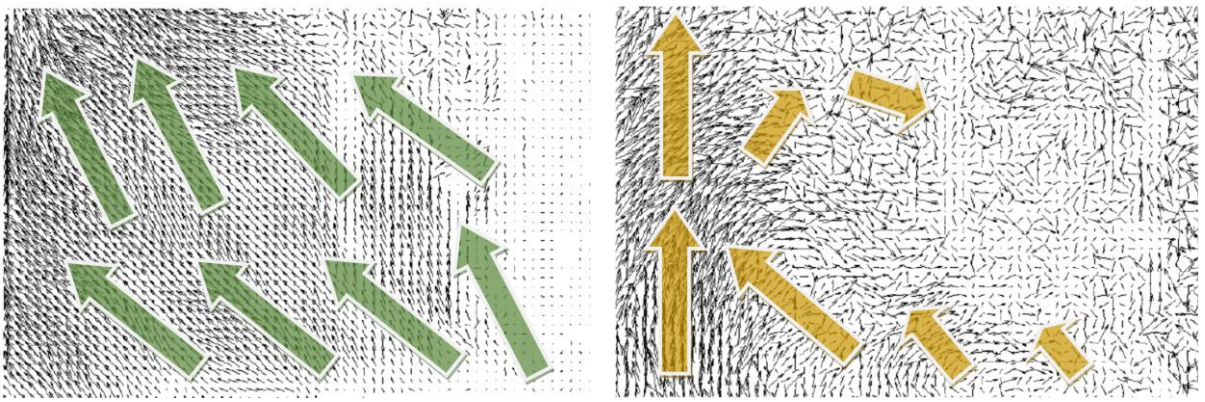

Fig. 9. Visualization of the flow field using the PIV measurements for two different icing states of the heat exchanger: (left) the heat exchanger is completely ice free – the flow is developed in the whole area pointing towards the left corner (fan); (right) the heat exchanger is severely blocked – the main flow direction is vertically from bottom to top on the left side, only small flow fields can develop in the right area.

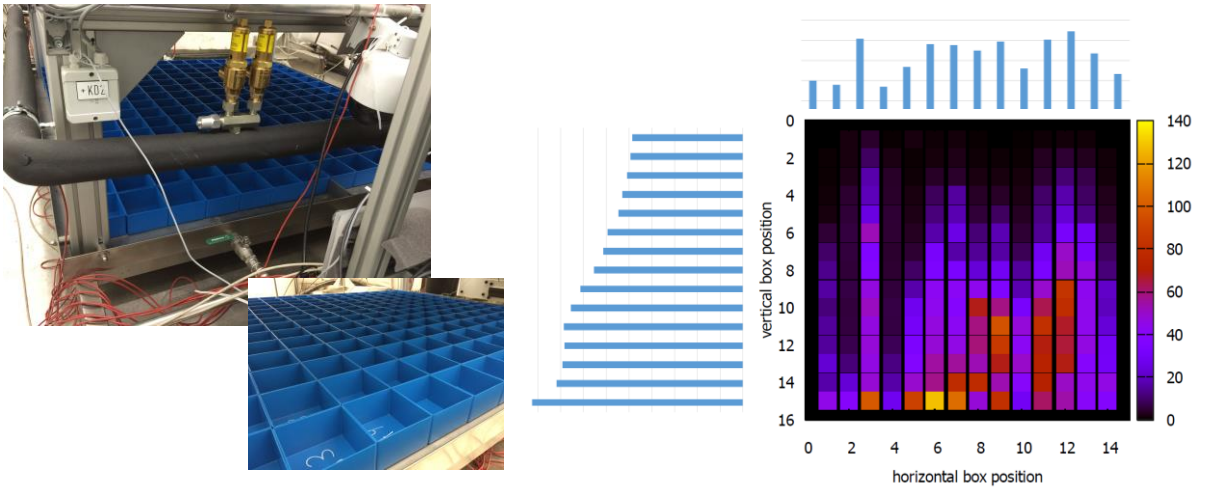

Fig. 10. (left) Collector boxes placed below the heat exchanger for collecting water during defrosting; (right) After defrosting, the locally collected water mass is visualized in [mg]. Sums over rows are shown on the left side using horizontal bars in [%], sums over columns shown on top in vertical bars in [%].

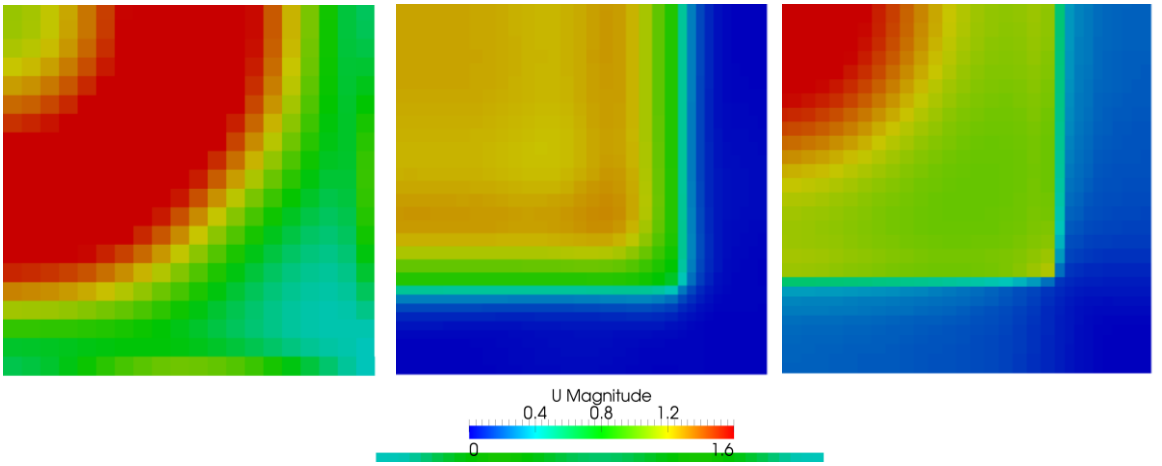

Fig. 11. Velocity magnitude [m/s] on different horizontal surfaces: (left) Surface 13 cm above the heat exchanger for reverse mode 90% fan control; (mid) 10 cm below the heat exchanger in normal mode at 60% fan control; (right) 10 cm below the heat exchanger in reverse mode at 60% fan control.

4. Conclusions

In the framework of the EU-project *GreenHP* (www.greenhp.eu), a characterization of the air side has been performed. Numerical and experimental techniques have shown, that the necessary air distribution through the heat exchanger at small power consumption of the fan and low noise emission could be reached. Computational fluid dynamics has been used to calculate the flow field inside the evaporator unit using the experimentally

acquired boundary conditions of the flow above the fan and below the heat exchanger. Utilizing advanced algorithms the simulation is able to predict ice onset during icing of the evaporator. The flow phenomena have been captured experimentally using laser optical techniques (PIV) and probe based methods (CTA), the accumulated ice mass has been additionally measured. We come to the following conclusions:

- Numerical and experimental analysis show that the main characteristics of the flow only changes slightly, when the rotational speed of the fan is changed from ~550 rpm (60% fan control) to ~1250 rpm (90% fan control). There is only an influence to the maximum of the achievable amplitudes.
- Large differences can be observed by changing the flow from normal to reversed mode. In normal mode homogenous distributions can be observed. In reverse mode, distinct turbulent flow patterns and shear layers can be seen as expected. They spread to the whole evaporator unit and extend even below the heat exchanger.

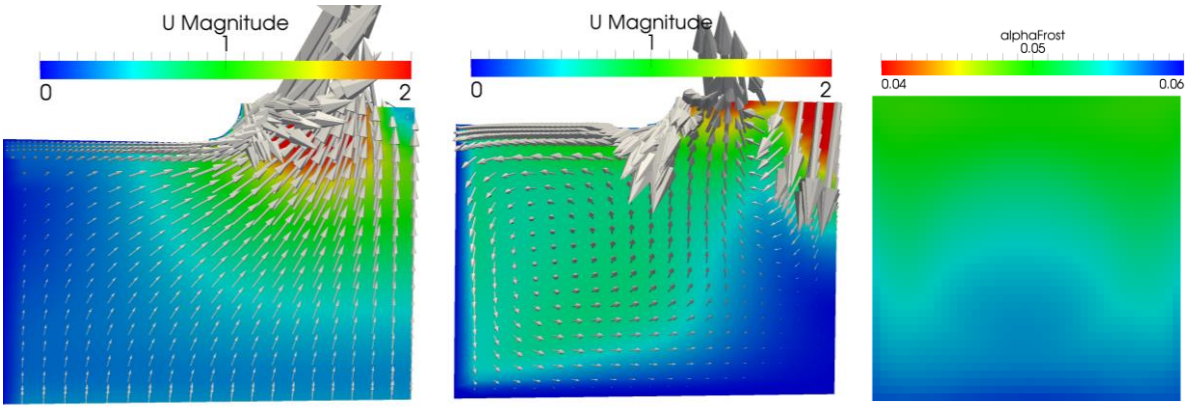

Fig. 12. (left) Contour and vector visualization of the CFD results for the normal mode with no icing; Visualization for the normal mode under severe icing conditions showing stalling flow and recirculation phenomena; (right) Simulated ice mass - *AlphaFrost* is a scalar representing the volume fraction occupied by the frost, which is calculated according to the frost growth model depending on the local flow (velocity and humidity) and frosting (temperatures of fluid and surface) conditions.

- The flow distribution inside of the unit (between heat exchanger and fan) is changing significantly during icing. In the clean (de-frosted) state a symmetric conic flow field showing only small recirculation zones is established. In the iced state, the blocked fins of the heat exchanger lead to a strongly directional flow field – a large part of the air volume only shows small flow velocities.
- Flow characteristics below the heat exchanger also differ depending on the operating mode in analogy to the findings inside of the unit. In normal mode a uniform air flow distribution can be observed.
- The ice (and water) distribution on the heat exchanger fins show an asymmetric pattern, which can be attributed to an inhomogeneous cooling media temperature and distribution, because the air flow field is homogenous.
- First, static pressure rise and sound power for two operating points have been measured for the fan in an anechoic room. A time-dependent acoustical analysis of the evaporator unit has been performed during icing in a climate chamber. The cooling circuit, compressor and air handling unit of the climate chamber have always been switched off for a short time to allow for recording the fan and heat exchanger only. Dependent on the position of the microphone a small increase in

sound pressure level has been detected at constant rotational speed of the fan. The corresponding frequency content of the acoustic signals show a small dependence on the microphone positions and small changes caused by icing. The introduction of two materials for sound shielding also caused only slight changes in overall sound emissions and frequency content.

Acknowledgements

This project is funded by the European Commission within the 7th Framework Programme (FP7) – grant agreement No FP7-Energy-2012-308816. Part of the work at AIT has also been performed supported by the Austrian Research Funding Agency (FFG) and Klima-Energy-Fonds (Project Numbers 82018, 829964, 834684).

References

[1] Strehlow A., Martín-Callizo C., Oltersdorf T., Popovac M., Reichl Ch., GreenHP: Heat Exchangers for Next Generation Heat Pump, 4th International Congress and Exhibition on Aluminium Heat Exchanger Technologies for HVAC&R, 10-11 June, 2015, Hotel Radisson Blu Scandinavia, Düsseldorf, Germany
[2] Reichl Ch., Strehlow A., Oltersdorf T., Braungardt S., Pröhl M., Benovsky P., Popovac M., Fleckl T., GreenHP: Next Generation Heat Pump for Retrofitting Buildings – new evaporator component for large capacity air-to-water heat pumps, Advanced HVAC & Natural Gas Technology Conference, May 6-9, 2015, Radisson BLU Hotel Latvija Conference Center, Riga, Latvia; DOI: 10.7250/rehvaconf.2015.015; page 100-109, 2015
[3] Crocker, M. J., (2004) Identification of noise sources on a residential split-system air-conditioner using sound intensity measurements, *Applied Acoustics* 65 (2004), p. 545-558
[4] Gustafsson, O. (2014), Flat tube heat exchangers – Direct and indirect noise levels in heat pump applications, *Applied Thermal Engineering* 66 (2014), p. 104-112, DOI: 10.1016/j.applthermaleng.2014.02.002
[5] Lörcher F., CFD-based fan optimization considering the system integration in a heat pump, Proceedings of Fan 2015 Symposium, Lyon, 2015
[6] Angelis A., Lörcher F., Fan unit with compact guide vane designed for low hub ratio axial fans, Proceeding of AMCA spring conference, San Antonio, 2015
[7] Weller H. G., Tabora G., Jasak H., Fureby C., A tensorial approach to computational continuum mechanics using object-oriented techniques, *Computers in Physics* 12: 620 – 631, 1998
[8] Na B., Webb R., A fundamental understanding of factors affecting frost nucleation, International Journal of Heat and Mass Transfer 46: 3797– 3808.
[9] Na B., Webb R., Mass transfer on and within a frost layer, *International Journal of Heat and Mass Transfer* 47: 899–911.
[10] Albert M., Sahinagic R., Gasser L., Wellig B., Hilfiker K., Prediciton of ice and frost deformation in the fin tube evaporators for Air/Water heat pump, 9th International IEA Heat Pump Conference, 2008
[11] Hermes C.J.L., Piucco R.O., Barbosa Jr. J.R.., Melo C., A study of frost growth and densification on flat surfaces, *Experimental Thermal and Fluid Science* 33: 371–379, 2009
[12] Popovac M., Seichter S., Benovsky P., Fleckl T., Reichl Ch., Numerical Analysis of the Frosting Performance of the air-side of a heat-pump, 24th IIR international congress of refrigeration, August 16-22, 2015, ICR2015, Yokohama, Japan
[13] Popovac M., Seichter S., Reichl C., Benovsky P., Implementation and application of the frost growth and densification model for numerical analysis of heat pump frosting performance. 6th IIR Conference: Ammonia and CO2 Refrigeration Technologies. Ohrid, FYRM.
[14] Reichl Ch., Seichter S., Popovac M., Benovsky P., Fleckl T., Experimentelle und numerische Methoden für die Untersuchung von Vereisung und Abtauverhalten von Verdampfern in Luftwärmepumpen, DKV Tagung 2014, Düsseldorf, Deutschland; 19.11.2014– 21.11.2014, in „Deutsche Kälte-Klimatagung 2014“